Applied Catalysis B: Environmental 163 (2015) 113–122

Contents lists available at ScienceDirect

Applied Catalysis B: Environmental

journal homepage: www.elsevier.com/locate/apcatb

Small CuO clusters on CeO_2 nanospheres as active species for catalytic N_2O decomposition

Maxim Zabilskiy[a], Petar Djinović[a], Boštjan Erjavec[a], Goran Dražić[b], Albin Pintar[a,*]

[a] Laboratory for Environmental Sciences and Engineering, National Institute of Chemistry, Hajdrihova 19, SI-1001 Ljubljana, Slovenia
[b] Laboratory for Materials Chemistry, National Institute of Chemistry, Hajdrihova 19, SI-1001 Ljubljana, Slovenia

ARTICLE INFO

Article history:
Received 16 June 2014
Received in revised form 21 July 2014
Accepted 25 July 2014
Available online 4 August 2014

Keywords:
N_2O decomposition
$CuO–CeO_2$ catalysts
Synergetic effect
Small CuO clusters
CeO_2 nanospheres

ABSTRACT

High surface area CeO_2 nanospheres as an active catalyst support were synthesized using glycothermal approach. Different loadings of copper (4, 6, 10 and 15 wt.%) were supported by wet impregnation method. Prepared materials were characterized by means of TEM, SEM-EDX, XRD, UV-Vis diffuse reflectance, N_2 adsorption/desorption, DRIFT and H_2-TPR techniques, and tested for the catalytic reaction of nitrous oxide decomposition. The best activity in the N_2O degradation was found for the sample containing 10 wt.% of Cu that can be attributed to the highest number of small CuO clusters on the catalyst surface. Further increase of copper content strongly affects the dispersion and leads to the formation of less active segregated CuO phase, which was confirmed by XRD, UV-Vis and H_2-TPR results. Accordingly to UV–Vis examination and DRIFT analysis using CO as a probe molecule, all solids contain Cu^{+1} ions which play a crucial role in the N_2O decomposition mechanism. The synthesized catalysts were also tested in wet or NO containing atmospheres, where an inhibiting effect takes place and leads to shifting of conversion profiles to higher temperature by 65 and 10 °C, correspondingly. It was found out that the formation of a new, crystalline $CuO{\cdot}3H_2O$ phase occurs in water vapour containing atmosphere, which can result in catalyst deactivation. However, this effect is fully reversible and the catalyst is able to replenish initial activity in dry atmosphere. Potentiality of CuO/CeO_2 materials in catalytic N_2O decomposition in industrial processes was confirmed by long-term stability tests performed in the period of 50 h in the presence of inhibiting gas components.

1. Introduction

Nitrous oxide (N_2O) is known as one of the strongest greenhouse gasses, due to its high global warming potential (310 times higher as compared to carbon dioxide), very long atmospheric lifetime (approx. 120 years) and its contribution to the destruction of ozone layer in the stratosphere [1]. Emissions of N_2O into atmosphere result in estimated accumulation of about 400 million tons of CO_2 equivalent annually [2]. Therefore, many efforts have been invested to evolve an efficient technology for N_2O removal from industrial exhaust gases. Nevertheless, development of a suitable catalyst for low temperature N_2O decomposition in the presence of water, oxygen and NO still remains a challenging task for environmental engineering.

Ceria (CeO_2) has been used as a catalyst or catalyst support in many catalytic processes due to its prominent redox properties, strong oxygen storage capacity and high oxygen mobility. Major technological applications of CeO_2 are catalysts for CO oxidation reaction, water gas shift reaction, NO reduction and automobile exhaust treatment [3]. Application of CeO_2 as a support or additive for N_2O degradation catalyst is also reported. Most publications are devoted to highly active catalysts containing Rh [4–8]. Kim et al. [4] reported that addition of ceria to an alumina support can significantly increase catalytic activity of Rh/Al_2O_3 materials. Parres-Esclapez et al. [5] underlined superior activity of Rh/CeO_2 catalyst in comparison to Rh/Al_2O_3 solid, and related this to the synergetic interaction between Rh and CeO_2 as well as to the participation of CeO_2 support in the N_2O decomposition mechanism, while γ-Al_2O_3 was acting as an inert carrier. Using La and Pr-doped CeO_2 supported Rh catalysts, it was possible to decrease half conversion temperature during N_2O decomposition experiments to 225 °C [6]. In spite of excellent catalytic properties of above-mentioned materials, it is highly unlikely that they will find industrial applications because of prohibitively high price of Rh. Therefore, development of a catalyst containing transition metals that are more preferential due to their low cost and high

* Corresponding author. Tel.: +386 1 47 60 237; fax: +386 1 47 60 460.
E-mail address: albin.pintar@ki.si (A. Pintar).

http://dx.doi.org/10.1016/j.apcatb.2014.07.057
0926-3373/

availability is a promising task towards the creation of a low temperature N_2O decomposition technology.

It was found that copper based materials can degrade nitrous oxide under elevated temperature. For example, Li et al. [9] reported that Cu exchanged ZSM-5 and mordenite are much more active than other cation-exchanged zeolites (Cu-Y, Co-Y, Co-erionite, Cu-L, Co-L, Ni-ZSM-5 and Mn-ZSM-5); however, activity of these solids is severely influenced by internal mass transfer limitations. Several works were aimed to study nitrous oxide decomposition over CuO supported on different carriers, such as SiO_2 [10], Al_2O_3 [10–12], carbon [10,13] and ZrO_2 [14]. Finally, interesting results of N_2O degradation over CuO–CeO_2 materials were reported [15,16].

Adamski et al. [15] studied an influence of preparation methods (i.e. impregnation, coprecipitation and coprecipitation-impregnation) on catalytic activity in both dry and wet streams. The authors stated that dimeric copper species possess weak catalytic activity in N_2O decomposition reaction due to their high tendency to accommodate oxygen intermediates produced during nitrous oxide degradation. It was stressed that the catalyst prepared by impregnation approach exhibits the highest activity in the reaction under consideration. However, no attention was paid to the examination of catalytic activity versus Cu loading. Zhou et al. [16] investigated N_2O activity dependence over catalysts with different loadings of Cu prepared by citrate method. It was discovered that a synergetic effect between CuO and CeO_2 promoted catalyst stability and ability to regenerate active sites. Results of catalytic tests further revealed that a sample containing 67 mol.% of Cu provided the highest N_2O conversion. Nevertheless, the above-mentioned CuO–CeO_2 materials exhibit low BET specific surface area (S_{BET} < 67 m^2/g), which suggests that further optimization of catalyst preparation techniques is still possible.

In this work, we investigated catalytic activity of CuO supported on high surface area (S_{BET} = 190 m^2/g) CeO_2 nanospheres, synthesized by means of advanced glycothermal approach. CuO/CeO_2 solids, with Cu content from 4 to 15 wt.%, were prepared by wet impregnation with aqueous $Cu(NO_3)_2$ and followed by calcination at 400 °C. The influence of Cu loading on redox, physical–chemical and catalytic properties was studied. To evaluate a contribution of different CuO species on catalytic N_2O decomposition, XRD, H_2-TPR, DRIFT and UV–Vis diffuse reflectance techniques were used. Finally, CuO/CeO_2 catalyst was tested in wet or NO containing atmospheres to evaluate inhibiting effects on reaction kinetics.

2. Experimental

2.1. Synthesis of CeO_2 powders by glycothermal method

Nanosized CeO_2 support was prepared using glycothermal approach [17]. The molar gel composition utilized during the synthesis was 1 $Ce(NO_3)_3$: 5.5 CH_3CH_2COOH: 220 $HOCH_2CH_2OH$. In a typical synthesis, 1.0 g of $Ce(NO_3)_3{\cdot}6H_2O$ (99% purity, Sigma–Aldrich) was dissolved in 1 ml of deionized water. Then, 30 ml of ethylene glycol (99.0% purity, Merck) and finally 1 ml of propionic acid (99% purity, Merck) were added under stirring to form a uniform solution. The mixed solution was transferred into a Teflon lined stainless steel autoclave and aged at different temperatures (140–180 °C) for 200 min under static conditions. After cooling to room temperature, 30 ml of acetone was added and the resulted suspension was centrifuged at 9000 rpm. The solid was then dried overnight and calcined at 400 °C in air. The prepared materials were marked as CeO_2-T (where *T* is a temperature utilized during the glycothermal treatment step, e.g. CeO_2-140).

To prepare CuO/CeO_2 catalysts with Cu content from 4 to 15 wt.%, wet impregnation approach was used. The CeO_2 support was impregnated with an aqueous solution of $Cu(NO_3)_2{\cdot}3H_2O$ (99.5% purity, Sigma–Aldrich) containing an appropriate amount of Cu. After overnight drying at room temperature, materials were calcined in nitrogen atmosphere at 400 °C for 3 h. Synthesized solids were marked as *X*-CuO/CeO_2-T (where *X* represents Cu content in wt.% accordingly to synthesis conditions).

2.2. Catalyst characterization

Determination of BET specific surface area, total pore volume and pore size distribution was performed at −196 °C using a TriStar II 3020 instrument from Micromeritics. The samples were degassed in N_2 stream (purity 6.0, Linde) at 300 °C for 3 h using the Micromeritics SmartPrep degasser. The Brunauer–Emmett–Teller (BET) method was applied for specific surface area calculations. The pore size distributions were derived from the desorption branch of the isotherms employing the Barrett–Joyner–Halenda (BJH) method. The total pore volume was estimated at a relative pressure of 0.989.

XRD patterns were recorded on a PANalytical X'pert PRO diffractometer equipped with the monochromator for Cu Kα1 radiation, λ = 0.15406 nm. Materials were scanned in the 2θ range between 10 and 85° with 0.0348° increments, respectively, and recording time of 100 s at each increment.

Temperature programmed reduction (TPR) experiments using H_2 were performed using a Micromeritics AutoChem II 2920 apparatus. 100 mg of a catalyst sample was calcined at 400 °C in synthetic air (20.5% O_2/N_2) and cooled to −20 °C. TPR analysis was performed in a 50 ml/min stream of 5% H_2/Ar mixture as a reducing agent. The samples were heated from −20 to 400 °C with a 5 °C/min ramp during analysis. A liquid nitrogen–isopropyl alcohol cold trap was mounted on exhaust in order to condense water vapour and remove it from the effluent gas mixture, before entering the TCD detector. Deconvolution of recorded TPR spectra was performed in Origin 8.1 software using Gaussian function.

UV–Vis diffuse reflectance spectra of CuO/CeO_2 catalysts were recorded at room temperature (RT) using a Perkin-Elmer Lambda 35 UV–Vis spectrophotometer equipped with the RSA-PE-19 M Praying Mantis accessory, which is designed for diffuse reflectance measurements of horizontally positioned powder samples, pastes or rough surface samples. Pure CeO_2-160 support was used to perform the instrument background correction in the range of 200–1100 nm. The scans were acquired with the speed of 120 nm min^{-1} and slit set to 4 nm.

The diffuse reflectance Fourier transform infrared (DRIFT) spectra were recorded in the range of 400–4000 cm^{-1} using a FT-IR analyzer (Perkin Elmer, model Frontier), equipped with a DRIFT cell and high temperature reaction chamber (Pike technologies), which allow to collect the spectra from RT to 900 °C. Before recording CO adsorption spectra, samples were pretreated in nitrogen at 300 °C for 30 min, and then cooled to RT under a nitrogen flow of 50 ml/min. Spectra were collected at RT with the resolution of 4 cm^{-1} and accumulation of 16 scans after treating in the flow of 1 vol.% CO/N_2 mixture for 10 min and followed by N_2 purging for 20 min.

The structural morphology of the prepared catalysts was studied using field-emission scanning electron microscope (Carl Zeiss, FE-SEM SUPRA 35VP), equipped with energy-dispersive X-ray spectroscopy hardware (Oxford Instruments, model INCA 400). Particle size, morphology and elemental mapping performed by EDXS analysis were investigated using Cs corrected scanning transmission electron microscope JEOL ARM 200 CF equipped with JEOL centurio 100 mm^2 EDXS system.

Table 1
Structural properties and results of screening tests for synthesized CeO_2 supports.

Sample	S_{BET} (m^2/g)	V_{pore} (cm^3/g)	[a]d_{pore} nm	[b]X(N_2O) (%)
CeO_2-140	151	0.25	2.4, 19.5	40
CeO_2-160	190	0.39	3.8, 44.1	54
CeO_2-180	112	0.14	1.8, 55.8	45

[a] Maxima of pore size distribution curves, calculated from desorption isotherms by the BJH method.
[b] $T = 400\,^{\circ}C$, catalyst weight 50 mg, feed flow rate 50 ml/min containing 2500 ppm N_2O in Ar. All the catalysts contained 6 wt.% of Cu.

2.3. Catalytic experiments

Catalytic N_2O decomposition experiments were performed in a fixed-bed quartz reactor. 50 mg of the tested material was diluted with 200 mg of inert SiC (BET specific surface area below 0.1 m^2/g) and positioned inside the 9 mm I.D. quartz tube and fixed between two quartz wool beads. Prior to experiments, the catalysts were activated in Ar flow (50 ml/min, purity 5.0, Messer) at 400 °C for 2 h. Degradation of nitrous oxide was performed at atmospheric pressure in the temperature range of 300–550 °C. N_2O feed concentration was 2500 ppm balanced by argon (Linde), while the gas feed flow rate was equal to 50 ml/min. At each examined temperature (set in intervals of 50 °C) the reaction was carried out for 30 minutes before measurements. The concentration measurements of reaction products and remaining N_2O at the reactor outlet were performed by gas chromatography using Agilent 490 Micro GC (Agilent Technologies) equipped with 10 m MS5A and 10 m Porabond Q columns. For catalytic experiments conducted in the inhibiting atmospheres, gas mixtures containing 2500 ppm of N_2O and either 1.5 vol.% of H_2O or NO balanced by argon were used. Long-term stability tests were carried out at 400 or 500 °C in inert or inhibiting atmospheres containing 2500 ppm N_2O.

3. Results and discussion

3.1. Characterization of CuO/CeO_2 materials

To determine optimal synthesis conditions for CeO_2 nanospheres, three temperatures, i.e. 140, 160 and 180 °C were utilized during the glycothermal preparation step. Results of nitrogen physisorption of synthesized solids are presented in Table 1, Figs. S1 and S2. One can see that different hydrothermal treatment temperatures greatly influence BET specific surface area of the prepared CeO_2 materials. CeO_2 with the highest specific surface area was obtained at the aging temperature of 160 °C. Further increase of glycothermal treatment temperature results in particle aggregation and consequently lower BET surface area and total pore volume. On the other hand, lower glycothermal temperature (140 °C) results in undeveloped mesoporous structure; because of this, BET specific surface area is about 40 m^2/g lower in comparison to the CeO_2-160 sample. High BET specific surface area of this solid suggests smaller crystallite size and highly defective structure, which are beneficial properties for utilizing this material as a support (possibility for higher dispersion of deposited active phase). Taking into account the above-mentioned facts and results of preliminary N_2O decomposition tests, where CeO_2-160 based catalyst (with 6 wt.% Cu loading) enabled 54% N_2O conversion at 400 °C, compared to 40 and 45% for CeO_2-140 and CeO_2-180 counterparts, respectively (see Table 1), we consequently selected the CeO_2-160 support for further catalyst preparation and all additional experiments.

Main physical–chemical properties of synthesized CuO/CeO_2 solids are summarized in Table 2. Chemical composition of examined samples was determined by means of SEM–EDX analyses. One can see that the actual weight contents of Cu are very close to the nominal values. The textural properties of the samples were studied by nitrogen physisorption. The type IV isotherms (Fig. S3) with hysteresis loop confirm the presence of mesopores, which are observed for all synthesized materials and appear to be very similar to the isotherm belonging to the CeO_2 carrier. With increasing Cu content we detected a decrease of BET specific surface area from 160 m^2/g for a sample containing 4 wt.% of Cu, to 133 m^2/g for a sample containing 15 wt.% of Cu. Also, the total pore volume of examined solids decreased somewhat, indicating that CuO nanoparticles were deposited within the CeO_2 nanospheres, resulting in partial blocking of the initially present pores. The materials exhibited bimodal pore size distribution with broad maxima centered at 3.8 and 26 nm, which are also present in CeO_2 nanospheres. The observed mesopores result from intergranular voids (the first maximum is related to voids between CeO_2 crystallites, while the second one to those between CeO_2 nanospheres).

SEM images of CeO_2-160 support and CuO/CeO_2 catalysts with various Cu loadings are presented in the Supplementary material in Figs. S4-9. The synthesized materials consist of nanospheres, which exhibit bimodal size distribution, i.e. being about 50 and 100 nm in diameter. The nanospheres are connected to each other and form larger aggregates with dimensions up to several micrometers. There are no distinguishable differences in morphology

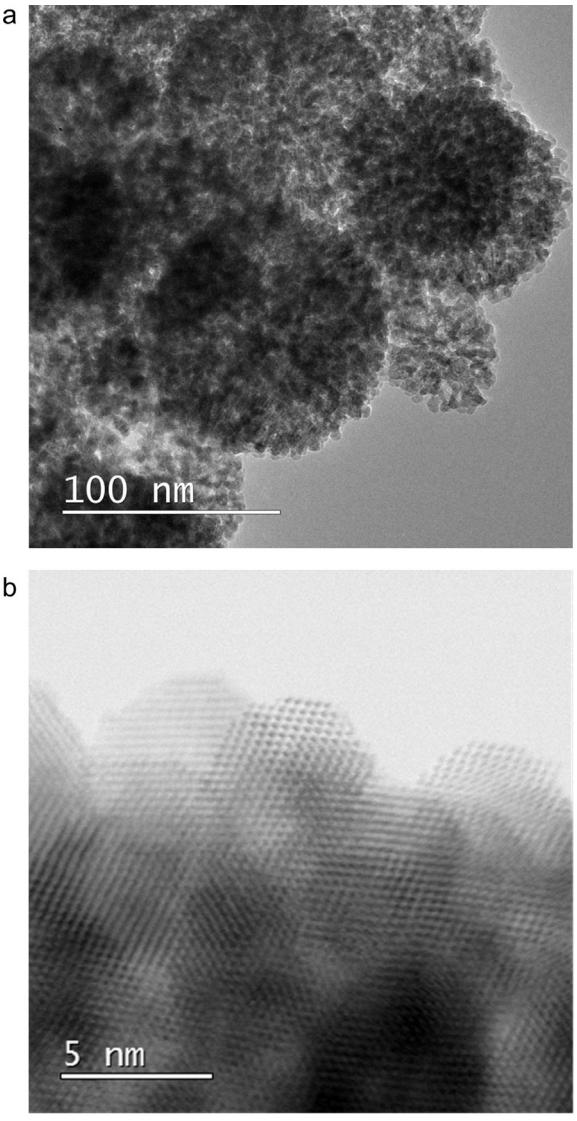

Fig. 1. TEM (a) and BF-STEM (b) images of 10-Cu/CeO_2-160 catalyst.

Table 2
Physical–chemical properties of synthesized CuO/CeO_2 catalysts.

Sample	[a]Cu content (wt.%)	[b]Cu content (wt.%)	S_{BET} (m^2/g)	V_{pore} (cm^3/g)	[c]Crystallite size of CeO_2 (nm)	[d]Crystallite size of CuO (nm)	[e]Lattice parameter (nm)
4-Cu/CeO_2-160	4	3.9	160	0.37	6.2	–	0.5420(4)
6-Cu/CeO_2-160	6	5.9	154	0.35		–	0.5414(5)
10-Cu/CeO_2-160	10	10.1	141	0.33		17	0.5408(4)
15-Cu/CeO_2-160	15	14.6	133	0.31		41	0.5407(5)

[a] Nominal loading.
[b] Measured by means of EDX analysis.
[c] Calculated by the Scherrer equation accordingly to the (1 1 1) diffraction peak of CeO_2.
[d] Calculated by the Scherrer equation accordingly to the (1 1 1) diffraction peak of CuO.
[e] For fluorite phase.

for catalysts with Cu loadings up to 10 wt.% (Figs. S5-7) and CeO_2 support (Fig. S4). Formation of CuO particles was not observed for these samples. 15-Cu/CeO_2-160 solid (Fig. S8) exhibits similar morphology to other samples and CeO_2 carrier itself, but during the detailed examination we also found CuO plate-like particles supported on CeO_2 nanospheres. As it can be seen in Fig. S9, large plates with dimensions up to 100 nm were detected, which can be attributed to the segregated CuO phase formed outside the CeO_2 nanospheres.

10-Cu/CeO_2-160 sample was additionally studied by means of TEM/STEM analysis. The results of this investigation, shown in Fig. 1, revealed that catalyst nanospheres further consist of smaller CeO_2 nanoparticles with dimensions from 5.2 to 6.3 nm. The elemental mapping images of energy dispersive X-ray (EDX) analysis

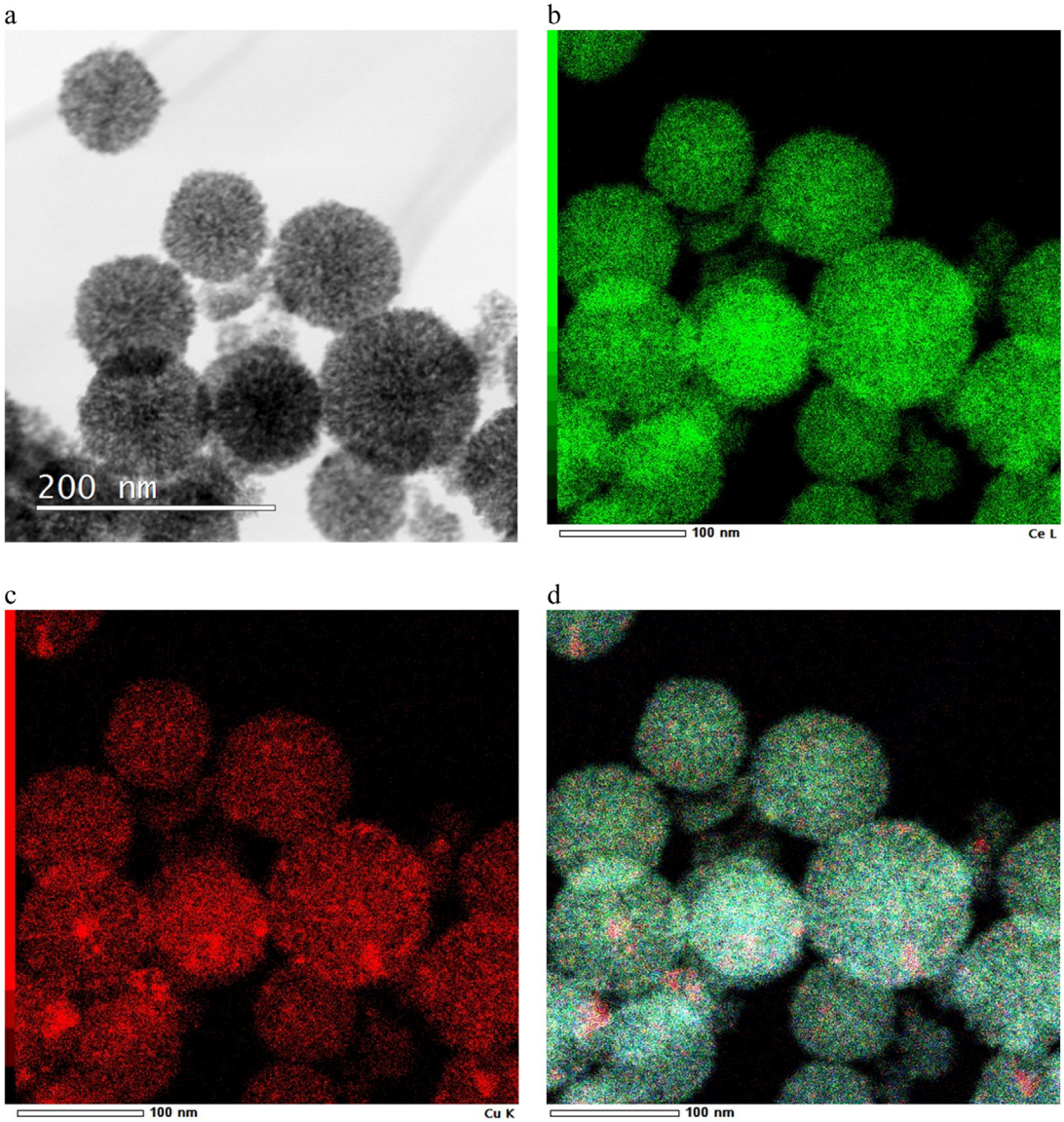

Fig. 2. BF-STEM image (a), elemental distribution of Ce (b) and Cu (c) as well as overlay of Ce and Cu distribution (d) observed by EDX spectroscopy for 10-Cu/CeO_2-160 catalyst.

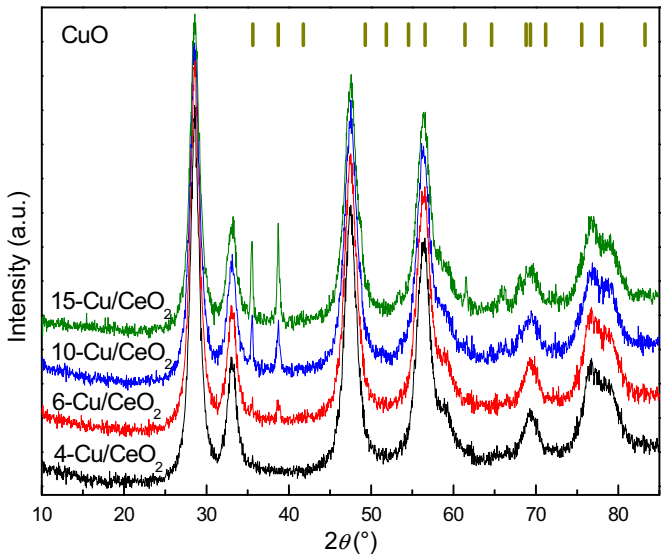

Fig. 3. XRD patterns of prepared CuO/CeO_2 catalysts.

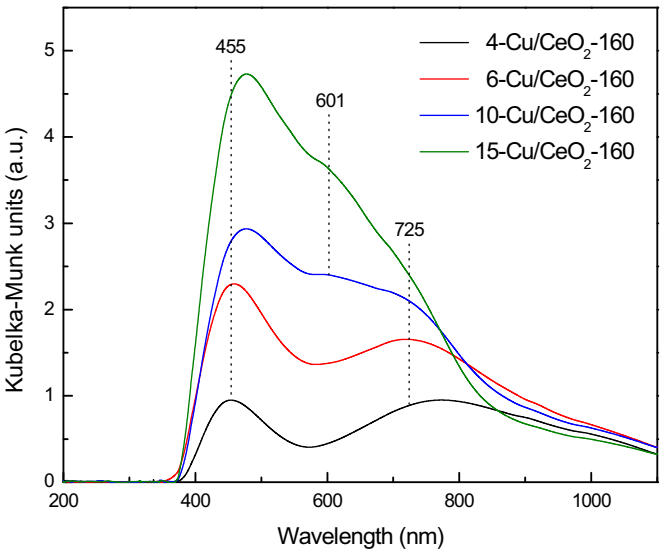

Fig. 4. UV–Vis diffuse reflectance spectra of prepared CuO/CeO_2 materials using CeO_2-160 as a reference standard.

(Fig. 2) showed that Ce is uniformly dispersed within the samples; however, copper is present as finely dispersed Cu, CuO clusters (less than 5 nm) and bulk CuO particles (up to 25 nm).

Formation of bulk CuO oxide at Cu loadings of 6–15 wt.% was also identified by XRD examination. The obtained XRD patterns of synthesized solids are illustrated in Fig. 3. The reflections from 4-CuO/CeO_2-160 sample can be assigned only to the FCC fluorite type of CeO_2 (PDF data file 03-065-5923). The absence of peaks belonging to any ordered copper containing phase can be explained by considering the fact that CuO particles are extremely small and well dispersed on the CeO_2 surface [18]. Samples containing from 6 to 15 wt.% of Cu displayed reflections from both FCC fluorite type of CeO_2 and monoclinic CuO tenorite phase (PDF data file 00-048-1548). Intensities of characteristic peaks at 35.49 and 38.73° belonging to monoclinic CuO phase significantly rise with increasing Cu loading, which is attributed to the formation of bulk CuO particles. The crystallite size of CuO calculated from (1 1 1) crystalline plane diffraction ($2\theta = 38.73°$) using the Scherrer equation is 17 and 41 nm for samples 10-CuO/CeO_2-160 and 15-CuO/CeO_2-160, respectively. However, calculated values do not take into account finely dispersed Cu and small CuO clusters, because XRD examination is not sensitive to small and non-crystalline particles; therefore, they represent an average size of CuO bulk phase only. The average CeO_2 crystallite size calculated from (1 1 1) crystalline plane diffraction ($2\theta = 28.59°$) using the Scherrer equation is 6.2 nm and equal for all investigated solids and CeO_2-160 support, which confirms good stability of ceria nanospheres and negligible extent of sintering during catalyst preparation steps.

UV–Vis diffuse reflectance spectra of investigated ceria supported CuO samples were recorded at room temperature using CeO_2-160 as a reference standard to perform the instrument background correction. Therefore, CeO_2 support does not contribute to the reflections and spectra shown in Fig. 4 are related to Cu containing species only. Three absorption bands can be detected at 455, 601 and 725 nm. The first absorption band most probably belongs to Cu^{+1} clusters and/or bis(μ-oxo)dicopper core ($[Cu_2O]^{2+}$). Praliaud et al. [19] observed an appearance of transition band at 450 nm during outgassing of alumina supported 6.4 wt.% of Cu at 773 K and ascribed it to the formation of three-dimensional Cu^{+1} clusters in the CuO matrix. He et al. [20] also assigned this peak to Cu^{+1} in CuO/CeO_2 solids and confirmed this by means of XPS analysis. However, Smeets et al. attributed peaks at 455 nm to the typical band of the bis(μ-oxo)dicopper core and believed that this type of Cu is active in catalytic N_2O decomposition [21].

Absorption band at 601 nm appeared for the 10-Cu/CeO_2-160 solid and further grew in intensity for 15-Cu/CeO_2-160 sample. Marion et al. [22] observed a strong absorption peak at 620 nm for bulk copper oxide, bulk CuO mechanically mixed with alumina and 9.2 wt.% CuO supported on alumina. Zhu et al. [11] also identified a band at 600 nm for CuO/Al_2O_3 sample calcined at 1200 °C. They noticed that this band disappears at lower calcination temperatures. This phenomenon was attributed to copper species, which are mainly present in the form of segregated CuO. Consequently, taking into account the observations of these investigators, the absorption band at 601 nm can be, with a high level of confidence, assigned to bulk CuO phase.

The band at 725 nm can be attributed to d–d Cu^{2+} transition in more or less tetragonally distorted O_h symmetry [19]. To conclude, the results of UV–Vis examination importantly show the presence of different Cu species (Cu^{+1}, Cu^{+2}) and formation of segregated CuO phase for samples with copper loading higher than 10 wt.%.

H_2-TPR analysis was used to investigate the reducibility of synthesized CuO/CeO_2 catalysts as well as to identify different Cu species present in the synthesized solids. Fig. 5 shows the derived H_2-TPR profiles and the corresponding fitting curves for prepared CuO/CeO_2 materials. Reduction of investigated catalysts was in all cases initiated at much lower temperatures in comparison to individual CuO and CeO_2 oxides, due to the so-called "synergetic effect" [23,24]. This effect is reported to originate from electronic interactions between the two phases, which weakens the M—O bonding and therefore enables reduction under milder conditions. Accordingly to the literature data, we can attribute the detected reduction peaks to the following processes: (i) reduction of finely dispersed Cu^{2+}, (ii) partial CeO_2 reduction, (iii) reduction of weak magnetic associates including several Cu^{2+} ions, (iv) reduction of small CuO clusters, and (v) reduction of bulk CuO [25–31].

For the 4-Cu/CeO_2-160 sample, three overlapping reduction peaks can be found, with maxima at 89 °C (denoted as peak α), 116 °C (denoted as peak β) and 137 °C (denoted as peak γ), respectively. Taking into account the results of UV–Vis diffuse reflectance and XRD examinations for this sample (note that no contribution could be observed for the segregated (bulk) CuO phase), the measured reduction peaks can be ascribed to highly dispersed or even atomically dispersed copper species. Accordingly to the literature

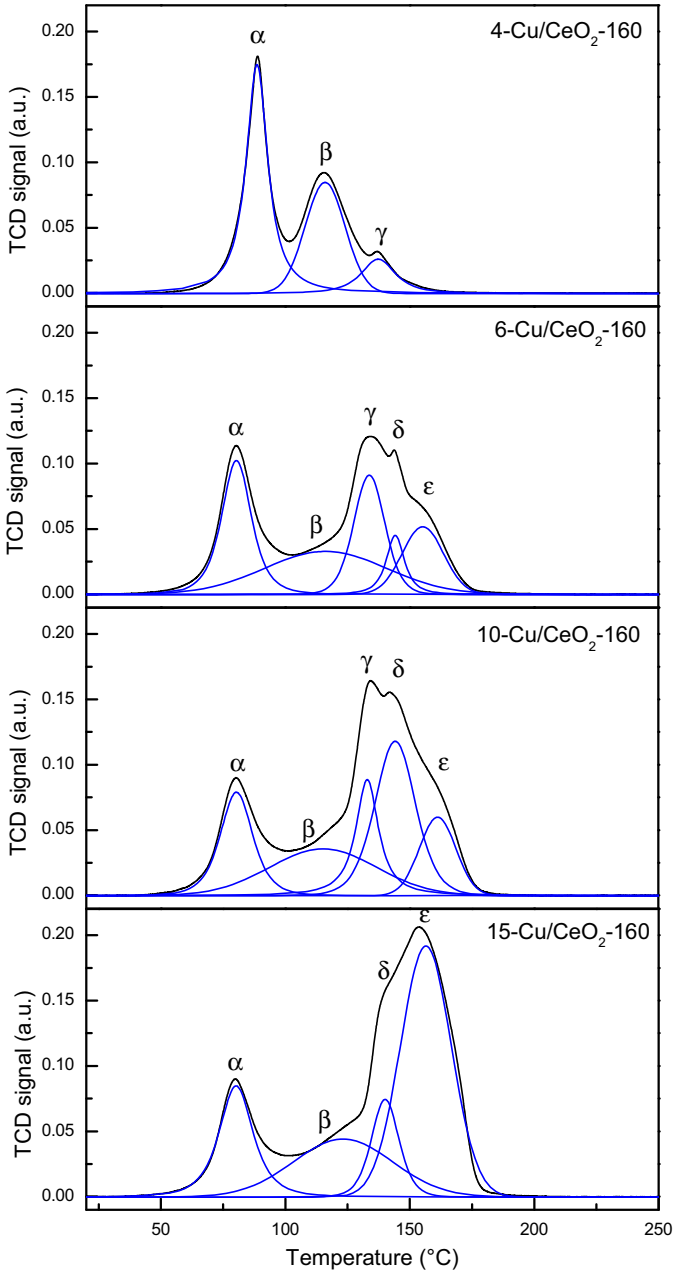

Fig. 5. H_2-TPR profiles of 4-Cu/CeO_2-160, 6-Cu/CeO_2-160, 10-Cu/CeO_2-160 and 15-Cu/CeO_2-160 catalyst samples.

data, the first reduction peak (α) corresponds to the reduction of finely dispersed Cu^{2+} strongly interacting with the CeO_2 support [25,26]. As it was stressed by Luo et al. [27], such kind of Cu species is easily reducible, since strong interaction with CeO_2 enhance CuO reducibility. The second peak (β) with a maximum at 116 °C most probably corresponds to a concurrent reduction of ceria [26]. Co-reduction of ceria at such low temperature can be explained by redox equilibria, which take place in CuO/CeO_2 mixed oxides: $Ce^{+4} + Cu^{+1} \leftrightarrow Cu^{+2} + Ce^{+3}$ and $Cu^0 + Ce^{+4} \leftrightarrow Ce^{+3} + Cu^{+1}$ [28,29]. Due to relatively slow oxygen diffusion from bulk to the surface of CeO_2, reduction rate is low and therefore the shape of this peak is broader in comparison to other reduction peaks (this is especially noticeable for samples with higher Cu content). The last peak present in the 4-Cu/CeO_2-160 sample can be assigned to reduction of weak magnetic associates including several Cu^{2+} ions, which contact closely with each other [26]. The presence of such kind of Cu species was confirmed by UV-Vis diffuse reflectance spectra (Fig. 4), where a peak at 455 nm can be attributed to the typical band of the bis(μ-oxo)dicopper core. Furthermore, Adamski et al. [15] and Martinez-Arias et al. [30] have verified the existence of Cu ionic pairs in CuO/CeO_2 materials by EPR investigations.

H_2-TPR spectra of samples with a higher copper content, besides the above-mentioned peaks, contain two additional peaks (δ and ε) with reduction maxima shifted to higher temperatures. With the increase of Cu loading, the intensity of ε peak raised significantly. Results of XRD and UV-Vis diffuse reflectance examinations indicate the formation of segregated CuO, therefore this peak with a maximum at 155–161 °C can be assigned to the reduction of bulk CuO phase, which is in agreement with the observations of other investigators [25–27,29,31]. Peak δ with a maximum at 140–144 °C is located between peaks assigned to the reduction of weak magnetic associates including several Cu^{2+} and bulk CuO phase. Considering this fact, we can reasonably assume that CuO particles, reduced at this temperature, should be smaller compared to bulk CuO particles, and larger than magnetic associates including several Cu^{2+}. Therefore, the peak located at 140–144 °C can be attributed to the reduction of small CuO clusters [26].

Results of H_2-TPR examinations are in good agreement with the results of HRTEM investigation, where we observed nonuniform CuO dispersion over CeO_2 nanospheres and formation of at least three different Cu species (finely dispersed Cu, CuO clusters and bulk CuO) for 10-Cu/CeO_2-160 solid. As one would expect, with increasing Cu content the growth of CuO particles takes place from highly dispersed CuO species, through small CuO clusters and finally to bulk CuO phase. The trend can be observed very clearly in Table 3 when comparing the relative contributions, obtained for each assigned type of CuO morphology with increasing CuO loading from 4 to 15 wt.%. In the 6-Cu/CeO_2-160 and 10-Cu/CeO_2-160 samples, the fraction of small CuO clusters grows from 7.5 to 30.3%, correspondingly, and decreases to 11.1% for the 15-Cu/CeO_2-160 sample. On the other hand, by comparing the same samples, H_2 consumed for the reduction of bulk CuO (ε peak) increases from 303 to 1374 $\mu mol/g_{cat}$. Finally, temperatures required for the reduction of synthesized CuO/CeO_2 nanocatalysts are considerably lower compared to commercially available CuO and CeO_2 powders and prepared CeO_2-160 support. Reduction of CeO_2-160 powder without deposited copper occurs at much higher temperature ($T > 400$ °C). This originates from substantially smaller particle size, abundance of defects and coordinatively unsaturated surface sites, which are highly reactive.

3.2. N_2O decomposition tests

Conversion of N_2O as a function of reaction temperature in the form of S-shaped curves is for the synthesized copper-ceria catalysts shown in Fig. 6. The measurements were done in duplicates and found to be reproducible. The most important observation is that catalytic activity increases with the rising content of deposited copper and reaches a maximum at 10 wt.% of Cu. Further increase of Cu loading (15-Cu/CeO_2-160 sample) led to a slightly lower catalytic activity in comparison to 10-Cu/CeO_2-160 material. In the given range of experimental conditions, total nitrous oxide conversion was reached at 550 °C for all the samples.

The observed differences in catalytic activity can be attributed to various CuO species present in the examined materials. Pure CeO_2 exhibits only minimal catalytic activity in the investigated temperature range (N_2O conversion below 10% at 400 °C). As it was discussed in the previous chapter, several types of copper species exist on the surface of CuO/CeO_2 solids and the relative proportion between these CuO species strongly depends on Cu loading (Table 3). With increasing copper content, CuO particles grow in size from predominantly finely dispersed Cu ions (82%, accordingly

Table 3
Comparison of the reducibility and H_2 consumption in TPR experiments for different catalysts.

Catalyst	[a]H_2 consumption ($\mu mol/g_{cat}$)					Total H_2 consumption ($\mu mol/g_{cat}$)
	α peak	β peak	γ peak	δ peak	ε peak	
4-Cu/CeO_2-160	747 (53.7; 89)	486 (34.9; 116)	159 (11.4; 138)			1392
6-Cu/CeO_2-160	484 (25.2; 80)	568 (29.7; 116)	418 (21.8; 134)	143 (7.5; 144)	303 (15.8; 155)	1916
10-Cu/CeO_2-160	407 (17.1; 80)	550 (23.0; 115)	393 (16.5; 133)	721 (30.3; 144)	313 (13.1; 161)	2384
15-Cu/CeO_2-160	473 (17.0; 80)	623 (22.4; 123)		308 (11.1; 140)	1374 (49.5; 157)	2778

[a] Numbers in parentheses represent mol.% of total H_2 consumption and peak position (°C), correspondingly.

to TPR results in Table 3 for 4-Cu/CeO_2-160 sample), through small CuO clusters (39% for 10-Cu/CeO_2-160 solid) and eventually to predominantly bulk CuO particles (64% for 15-Cu/CeO_2-160 material). This was calculated based on the relative amount of H_2 spent for reduction of these individual CuO morphologies, compared to the total H_2 amount consumed for complete CuO reduction. Interestingly, sample 4-Cu/CeO_2-160 exhibiting the highest content of most easily reducible and finely dispersed CuO, which should supposedly be very active, revealed inferior catalytic activity among the tested catalysts. A simple explanation of this phenomenon can be provided upon considering N_2O decomposition mechanism over catalysts containing Cu^{+1} active sites. The presence of the latter in the investigated CuO/CeO_2 solids was confirmed by UV–Vis diffuse reflectance examination (absorption peak at 450 nm) and DRIFT spectroscopy using CO as a probe molecule (see Fig. 7). In DRIFT experiments all tested materials were pre-activated at 400 °C in nitrogen (temperature at which all the catalysts are active in the examined reaction; N_2O conversion is in the range of 35–60%) and cooled to RT. After CO adsorption a strong band at 2107 cm^{-1} appears in the spectra, which can be ascribed to the Cu^{+1}–CO complex. A shoulder at 2059 cm^{-1} can be most likely attributed to carbonyl species adsorbed on metallic copper [30]. As it was reported [10,11,16], N_2O molecule interacts and adsorbs on Cu^{+1} site via oxygen (Eq. (1)). Such interaction leads to weakening of N—O bond, followed by N_2 desorption and oxidation of Cu^{+1} to Cu^{+2} (Eq. (2)).

$$Cu^{+1} + ONN \rightarrow Cu^{+1}\text{–}ONN \quad (1)$$

$$Cu^{+1}\text{–}ONN \rightarrow Cu^{+2}\text{–}O^{-} + N_2 \quad (2)$$

$$Cu^{+2}\text{–}O^{-} \rightarrow 2Cu^{+1} + O_2 \quad (3)$$

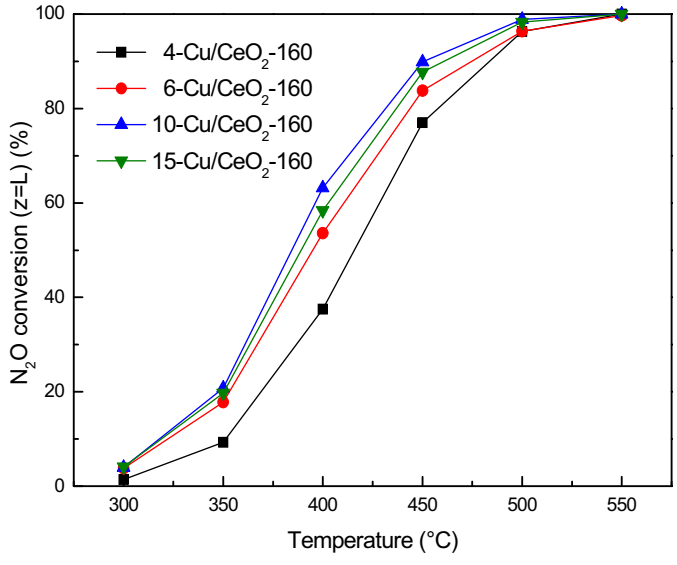

Fig. 6. N_2O conversion as a function of reaction temperature for CuO/CeO_2 catalysts (WHSV = 60 L/(g_{cat} h)).

To regenerate the initial Cu^{+1} active sites, the oxygen recombination step needs to occur, followed by desorption of molecular oxygen. This step is rapid only on two neighbouring Cu^{+2}—O^{-} sites, which enable the two proximal adsorbed oxygen atoms to directly combine and to form an oxygen molecule (Eq. (3)).

In the case of isolated Cu^{+2}—O^{-} sites (predominantly atomically dispersed Cu phase is present in 4-Cu/CeO_2-160 catalyst), the recombination step described above is severely hindered. As a consequence, the Cu^{1+} active sites can be regenerated by coupling with mobile oxygen species originating from the reducible CeO_2 support, followed by desorption of molecular oxygen. This is the reason why catalysts containing mainly easily reducible and atomically dispersed Cu species exhibit inferior activity during the nitrous oxide degradation reaction.

As mentioned before, with further increasing copper content the growth of average CuO particle size takes place. Accordingly to H_2-TPR examination (Fig. 5 and Table 3), the sample containing 10 wt.% of Cu exhibits the largest number of small CuO clusters (δ reduction peak) among the prepared CuO/CeO_2 solids. We observed a good correlation between the amount of small CuO clusters and activity in N_2O decomposition reaction, so we can reasonably conclude that such CuO particles (with a diameter below 5 nm, as determined by TEM analysis) contribute most to the observed catalytic activity. Further increase of copper loading (sample 15-Cu/CeO_2-160) results in the formation of segregated and less active CuO phase (bulk CuO), which was confirmed by means of XRD, SEM, UV-Vis and H_2-TPR investigations. At the same time, the number of small CuO clusters decreased in comparison to the sample containing 10 wt.% of Cu (Fig. 5 and Table 3), which in turn resulted in lower catalytic activity. Bulk CuO phase (particle size of about 41 nm, as identified by means of XRD technique) is less reactive towards N_2O decomposition as it contains a lower amount of structural defects and other high-energy, coordinatively unsaturated reactive sites.

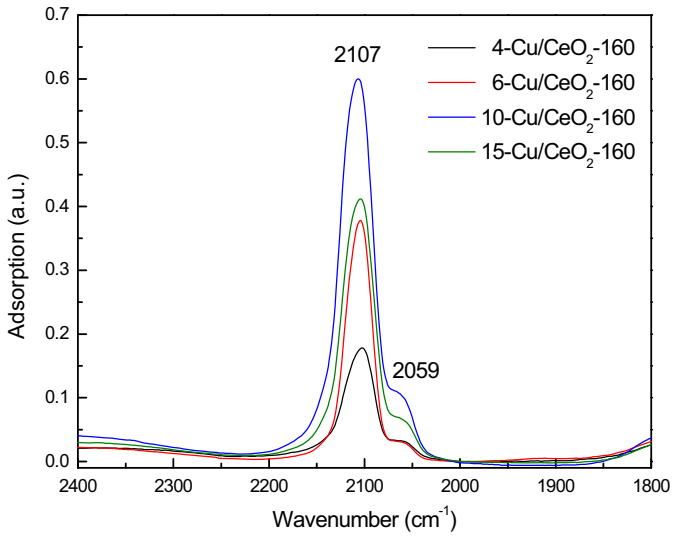

Fig. 7. DRIFT spectra of synthesized CuO/CeO_2 solids using CO as a probe molecule.

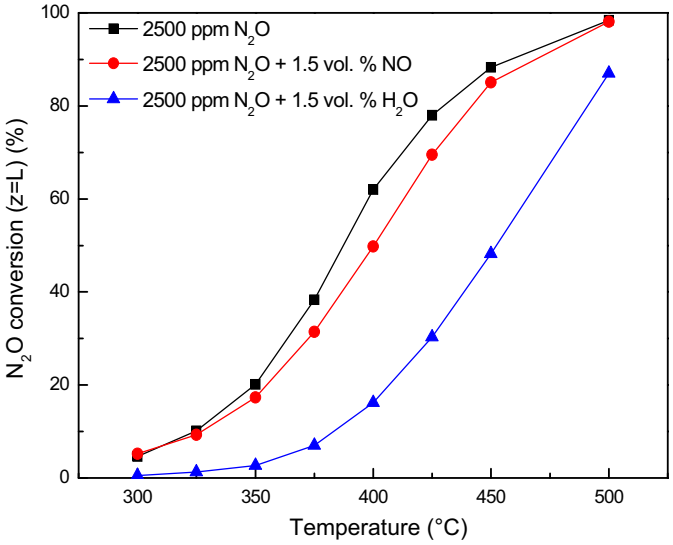

Fig. 8. Catalytic N_2O decomposition as a function of reaction temperature over 10-Cu/CeO_2-160 sample under different reaction atmospheres (WHSV = 60 L/(g_{cat} h)).

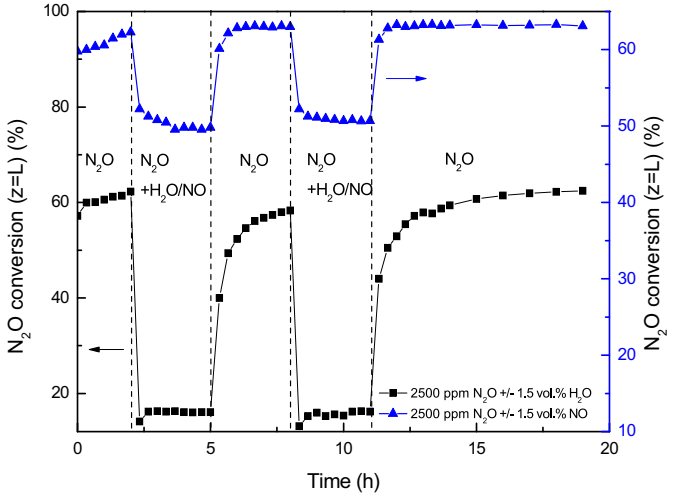

Fig. 9. Catalytic N_2O decomposition during step change experiment over 10-Cu/CeO_2-160 sample at reaction temperature of 400 °C and WHSV = 60 L/(g_{cat} h)).

Also, electronic and other interactions between CuO clusters and CeO_2 support (synergetic effect) are less pronounced when the two phases are not in an intimate contact with a substantial interfacial surface area.

Table 4 presents a comparison of catalytic N_2O decomposition results over CuO/CeO_2 solids investigated in this work and over the catalysts utilized by other research groups [6,15,16,32,33]. As one can see, 10-CuO/CeO_2-160 catalyst showed the highest activity during catalytic N_2O degradation among CuO/CeO_2 based materials. Zhou et al. [16] reported half conversion temperature (T_{50}) of about 370 °C utilizing GHSV = 19000 h^{-1}. We observed almost the same T_{50} value (380 °C), however, GHSV and N_2O feed concentration were two times higher (GHSV = 45000 h^{-1}), which allows us to conclude that the activity of the 10-CuO/CeO_2-160 catalyst was higher. It is worth to notice that 0.5 wt.% Pt/Al_2O_3 + CeO_2 + La_2O_3 catalyst [33] shows very similar half conversion temperature – 360 °C (GHSV = 12 000 h^{-1}, [N_2O] = 1000 ppm); therefore, we can achieve comparable results utilizing Cu instead of Pt, which is considerably more expensive.

The effects of H_2O and NO in the reactant feed on N_2O conversion were investigated in the presence of 10-Cu/CeO_2-160 sample, which exhibits the highest activity in catalytic nitrous oxide degradation reaction (Fig. 6). These two components are usually present in N_2O-containing gas streams intended for catalytic treatment before being discharged into the atmosphere. Fig. 8 shows results of N_2O decomposition under model atmosphere (2500 ppm N_2O diluted in argon) and atmospheres additionally containing either NO (1.5 vol.%) or H_2O (1.5 vol.%). The presence of NO in the gas stream together with N_2O slightly decreased the catalytic activity and resulted in minor effect in nitrous oxide conversion; half conversion temperature increased for 10 °C. In contrast to NO, the inhibiting effect of H_2O vapour present in the feed stream was much stronger. The activity of examined catalyst decreased in the presence of water, which in turn increased T_{50} for about 65 °C. Drop of catalytic activity under wet and NO containing atmosphere is a well-known fact not only for CuO/CeO_2 solids [15], but also for other catalytic systems [33–36]. The main reason for this phenomenon is concurrent adsorption of NO and H_2O, and blockage of active catalytic sites.

This inhibiting effect was additionally studied in the present work through a step-change experiment, where the feed composition was switched periodically between gas mixtures containing 2500 ppm N_2O in argon, or N_2O/Ar and 1.5 vol.% of H_2O or NO. The results of this experiment (Fig. 9) indicate a completely reversible character of H_2O/NO poisoning. The catalyst regenerates initial activity in 1 h after exposure to NO, or in 5 h after being exposed to water. Greater influence of H_2O on catalytic activity and much longer regeneration time after water poisoning can be attributed not only to co-adsorption of water on the catalyst surface, but also to the formation of a new, crystalline copper containing phase. Fig. 10 represents XRD patterns of samples that have been exposed to 500 °C in atmosphere containing only 2500 ppm N_2O in argon (dry conditions), and atmosphere additionally containing 1.5 vol.% H_2O. The diffractogram of the sample operated in wet conditions exhibits an additional reflection at $2\theta = 34.14°$, which corresponds to the most intensive reflection of CuO·$3H_2O$ phase (PDF data file 00-036-0545). Therefore, re-establishment of initial catalytic activity is slower, as decomposition of this phase and recrystallization to the originally present CuO clusters is required for complete regeneration of catalytic activity.

In order to estimate the potential of CuO/CeO_2 materials in catalytic N_2O decomposition in industrial processes, long-term stability tests were performed in the presence of most active

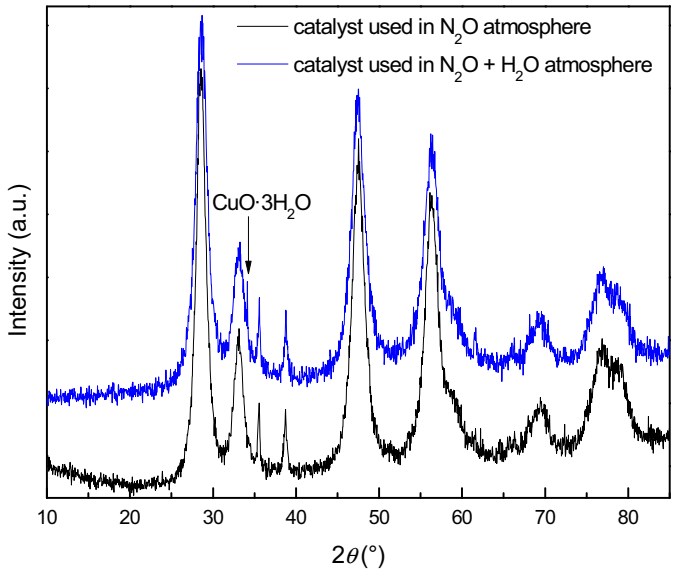

Fig. 10. XRD patterns of spent 10-Cu/CeO_2-160 catalyst samples.

Table 4
Comparison of N_2O decomposition over 10-CuO/CeO_2-160 material and catalysts utilized in other works.

Catalyst (metal loading)	T_{50} (°C)[a]	Experimental conditions during catalytic test	Ref.
CuO/CeO_2 (5 mol.% of Cu)	430	350 mg of the catalyst, $[N_2O]$ = 50 000 ppm, 30 ml/min	[15]
CuO/CeO_2 (67 mol.% of Cu)	370	GHSV = 19 000 h^{-1}, $[N_2O]$ = 2600 ppm	[16]
CuO/CeO_2 (40 mol.% of Cu)	440	GHSV = 45 000 h^{-1}, $[N_2O]$ = 2500 ppm	[32]
$Pt/Al_2O_3 + CeO_2 + La_2O_3$ (0.5 wt.% of Pt)	365	GHSV = 10 000 h^{-1}, $[N_2O]$ = 1000 ppm	[33]
$Rh/CeO_2 + La_2O_3$ (0.5 wt.% of Rh)	225	GHSV = 12 000 h^{-1}, $[N_2O]$ = 1000 ppm	[6]
10-CuO/CeO_2-160 (10 wt.% of Cu)	380	GHSV = 45 000 h^{-1}, $[N_2O]$ = 2500 ppm (50 mg of the catalyst, 50 ml/min)	Present work

[a] Half conversion temperature (T_{50}).

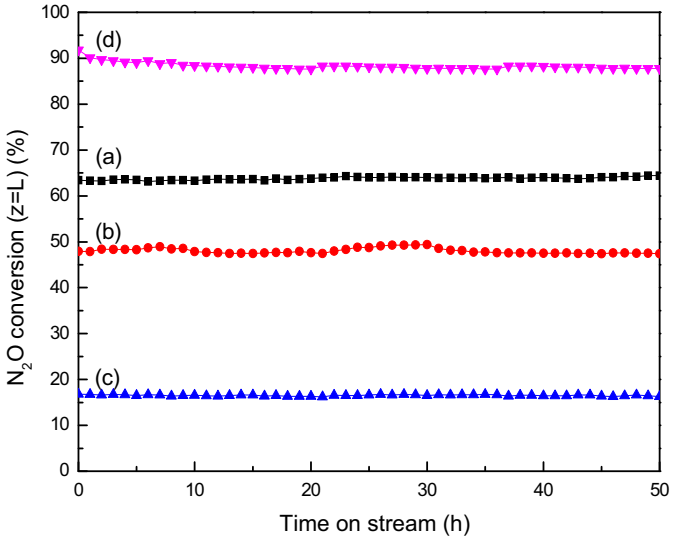

Fig. 11. N_2O conversion measured as a function of time on stream for 10-Cu/CeO_2-160 sample under different reaction conditions: (a) 2500 ppm N_2O, WHSV = 60 L/(g_{cat} h), 400 °C; (b) 2500 ppm N_2O + 1.5 vol.% NO, WHSV = 60 L/(g_{cat} h), 400 °C; (c) 2500 ppm N_2O + 1.5 vol.% H_2O, WHSV = 60 L/(g_{cat} h), 400 °C; (d) 2500 ppm N_2O + 1.5 vol.% H_2O, WHSV = 30 L/(g_{cat} h), 500 °C.

10-Cu/CeO_2-160 catalyst. These tests were carried out at T = 400 °C under model atmosphere (2500 ppm N_2O diluted in argon) and atmospheres containing either 1.5 vol.% NO or H_2O (Fig. 11). As one can see, no significant changes in catalytic activity as a function of time on stream were observed. The obtained data clearly demonstrate that the CeO_2 supported CuO catalyst was stable at 400 °C and able to regenerate the active Cu^{+1} sites by desorption of formed oxygen from oxidized Cu^{2+} sites even in the inhibiting atmospheres. Addition of NO and H_2O to the N_2O feed stream resulted in a relative drop of N_2O space time yield (STY) for 17 and 48%, respectively. Structural stability and prevention of catalyst sintering during the long-term stability tests were also confirmed by results of nitrogen physisorption and XRD examination of spent catalysts, where changes in BET specific surface area and crystallite size of CuO and CeO_2 were found to be negligible. Finally, the 10-Cu/CeO_2-160 catalyst was tested in wet atmosphere at 500 °C (Fig. 11, run d) where catalyst sintering and deactivation were expected to be more intensive. After the initial period of 10 h, in which we observed a decrease in N_2O conversion from 91 to 88%, the synthesized catalyst showed stable performance. These results undoubtedly highlight the outstanding catalytic activity and stability of examined CuO/CeO_2 catalyst, and open the way to further investigation and enhancement of this catalytic system.

4. Conclusions

In this study, a series of CuO supported on CeO_2 nanospheres were investigated in catalytic N_2O decomposition. Synthesized solids contained from 4 to 15 wt.% of copper and exhibited high BET specific surface area (133–160 m^2/g). Cu loading greatly influenced the physical-chemical, redox and catalytic properties of investigated solids. Accordingly to the results of H_2-TPR, TEM and UV–Vis diffuse reflectance analyses, several copper species are present on the surface of CuO/CeO_2 oxides. By increasing copper loading from 4 to 15 wt.%, the growth of CuO particles from highly dispersed Cu species, through small CuO clusters and finally to bulk CuO phase takes place.

We have shown that CuO/CeO_2 catalysts exhibit very promising activity and stability to be effectively applied in catalytic N_2O decomposition. The highest activity is observed for the 10-CuO/CeO_2-160 material containing 10 wt.% of Cu, which has the highest amount of small CuO clusters. These clusters are less than 5 nm in size and represent 39% of the total CuO amount in the 10-CuO/CeO_2-160 catalyst. This was calculated based on the relative amount of H_2 spent for reduction of these clusters, compared to the total H_2 amount required for CuO reduction. It is therefore assumed that this morphology contributes significantly to the observed N_2O conversions. Further increase of Cu loading to 15 wt.% results in the formation of segregated and less active bulk CuO phase. The presence of NO and water vapour exhibits a detrimental effect on the catalytic activity, as these species adsorb and block the active sites. The negative effect of water vapour is more pronounced, as it also causes restructuring of CuO to $CuO{\cdot}3H_2O$. Regeneration of CuO/CeO_2 catalysts in diluted N_2O stream is fully reversible, but is slower in the case of co-fed water, which is due to the decomposition of $CuO{\cdot}3H_2O$ phase. Good performance and no deactivation of the catalyst containing 10 wt.% of Cu, even in NO and water vapour containing atmospheres, was confirmed by 50-h stability tests.

Acknowledgements

The authors gratefully acknowledge the financial support of the Ministry of Education, Science and Sport of the Republic of Slovenia through Research program P2-0150.

Appendix A. Supplementary data

Supplementary data associated with this article can be found, in the online version, at http://dx.doi.org/10.1016/j.apcatb.2014.07.057.

References

[1] http://epa.gov/climatechange/ghgemissions/gases/n2o.html, accessed 13.06.2014.
[2] http://www.state.gov/e/oes/rls/rpts/car4/90324.htm, accessed 13.06.2014.
[3] A. Trovarelli, Catalysis by Ceria and Related Materials, Imperial College Press, London, 2002, pp. 508.
[4] S.S. Kim, S.J. Lee, S.C. Hong, Chem. Eng. J. 169 (2011) 173.
[5] S. Parres-Esclapez, I. Such-Basanez, M.J. Illán-Gómez, C. Salinas-Martínez de Lecea, A. Bueno-López, J. Catal. 276 (2010) 390.
[6] A. Bueno-López, I. Such-Basanez, C. Salinas-Martínez de Lecea, J. Catal. 244 (2006) 102.
[7] S. Imamura, J. Tadani, Y. Saito, Y. Okamoto, H. Jindai, C. Kaito, Appl. Catal. A 201 (2000) 121.
[8] M. Inger, M. Wilk, S. Parres-Esclapez, M.J. Illán-Gómez, C. Salinas-Martínez de Lecea, A. Bueno-López, J. Chem. Technol. Biotechnol. 88 (2013) 2233.

[9] Y. Li, J.N. Armor, Appl. Catal. B 1 (1992) L21.
[10] A. Dandekar, M.A. Vannice, Appl. Catal. B 22 (1999) 179.
[11] Z.H. Zhu, H.Y. Zhu, S.B. Wang, G.Q. Lu, Catal. Lett. 91 (2003) 73.
[12] K.W. Yao, S. Jaenicke, J.Y. Lin, K.L. Tan, Appl. Catal. B 16 (1998) 291.
[13] J. Ma, N.M. Rodriguez, M.A. Vannice, R.T.K. Baker, Topics Catal. 10 (2000) 27.
[14] C. Morterra, E. Giamello, G. Cerrato, G. Centi, S. Perathoner, J. Catal. 179 (1998) 111.
[15] A. Adamski, W. Zając, F. Zasada, Z. Sojka, Catal. Today 191 (2012) 129.
[16] H. Zhou, Z. Huang, C. Sun, F. Qin, D. Xiong, W. Shen, H. Xu, Appl. Catal. B 125 (2012) 492.
[17] X. Liang, J. Xiao, B. Chen, Y. Li, Inorg. Chem. 49 (2010) 8188.
[18] P. Djinović, J. Batista, A. Pintar, Catal. Today 147S (2009) S191.
[19] H. Praliaud, S. Mikhailenko, Z. Chajar, M. Primet, Appl. Catal. B 16 (1998) 359.
[20] C. He, Y. Yu, L. Yue, N. Qiao, J. Li, Q. Shen, W. Yu, J. Chen, Z. Hao, Appl. Catal. B 147 (2014) 156.
[21] P.J. Smeets, M.H. Groothaert, R.M. van Teeffelen, H. Leeman, E.J.M. Hensen, R.A. Schoonheydt, J. Catal. 245 (2007) 358.
[22] M.C. Marion, E. Garbowski, M. Primet, J. Chem. Soc. Farad. Trans. 86 (1990) 3027.
[23] K. Zhou, R. Xu, X. Sun, H. Chen, Q. Tian, D. Shen, Y. Li, Catal. Lett. 101 (2005) 169.
[24] J. Chen, Y. Zhan, J. Zhu, C. Chen, X. Lin, Q. Zheng, Appl. Catal. A 377 (2010) 121.
[25] Y. Zhang, C. Chen, X. Lin, D. Li, X. Chen, Y. Zhan, Q. Zheng, Int. J. Hydrogen Energ. 39 (2014) 3746.
[26] X. Yao, F. Gao, Q. Yu, L. Qi, C. Tang, L. Dong, Y. Chen, Catal. Sci. Technol. 3 (2013) 1355.
[27] M.F. Luo, Y.P. Song, J.Q. Lu, X.Y. Wang, Z.Y. Pu, J. Phys. Chem. C 111 (2007) 12686.
[28] C. Lamonier, A. Ponchel, A. D'Huysser, L. Jalowiecki-Duhamel, Catal. Today 50 (1999) 247.
[29] R. Si, J. Raitano, N. Yi, L. Zhang, S.W. Chan, M. Flytzani-Stephanopoulos, Catal. Today 180 (2012) 68.
[30] A. Martinez-Arias, M. Fernández-García, J. Soria, J.C. Conesa, J. Catal. 182 (1999) 367.
[31] J.L. Ayastuy, A. Gurbani, M.P. González-Marcos, M.A. Gutiérrez-Ortiz, Ind. Eng. Chem. Res. 48 (2009) 5633.
[32] M. Zabilskiy, B. Erjavec, P. Djinović, A. Pintar, Chem. Eng. J. 254 (2014) 153.
[33] M. Konsolakis, F. Aligizou, G. Goula, I.V. Yentekakis, Chem. Eng. J. 230 (2013) 286.
[34] S. Parres-Esclapez, M.J. Illán-Gómez, C. Salinas-Martínez de Lecea, A. Bueno-López, Int. J. Greenh. Gas Control 11 (2012) 251.
[35] P.J. Smeets, B.F. Sels, R.M. van Teeffelen, H. Leeman, E.J.M. Hensen, R.A. Schoonheydt, J. Catal. 256 (2008) 183.
[36] M. Santiago, J. Pérez-Ramírez, Environ. Sci. Technol. 41 (2007) 1704.